Electronic Supplementary Material (ESI) for Inorganic Chemistry Frontiers.

Supporting Information

Light-induced disruption of an acyl hydrazone link as a novel strategy for drug release and activation: isoniazid as a proof-of-concept case

Authors: Edinaira Deodato Nunes[a], Anne Drumond Villela[b,c], Luiz Augusto Basso[b,c], Edson H. Teixeira[d], Alexandre L. Andrade[d], Mayron A. Vasconcelos[d,e], Luiz G. do Nascimento Neto[d,f], Ana C. S. Gondim[a], Izaura C. N. Diógenes[a], Adolfo I. B. Romo[a], Otaciro R. Nascimento[g], Davila Zampieri[h], Tércio Freitas Paulo[a], Idalina Maria Moreira de Carvalho[a], Luiz Gonzaga de França Lopes[a,b], Eduardo H. S. Sousa[a,b]*

[a] Laboratório de Bioinorgânica, Departamento de Química Orgânica e Inorgânica, Universidade Federal do Ceará, CEP 60455-760, Fortaleza, Ceará, Brazil.

[b] Instituto Nacional de Ciência e Tecnologia em Tuberculose, Pontifícia Universidade Católica do Rio Grande do Sul, Porto Alegre, Brazil

[c] Pontifícia Universidade Católica do Rio Grande do Sul, Centro de Pesquisas em Biologia Molecular e Funcional, Av Ipiranga 6681, Porto Alegre, RS 90619-900, Brazil

[d] Laboratório Integrado de Biomoléculas, Departamento de Patologia e Medicina Legal, Universidade Federal do Ceará, 60441−750
Fortaleza, Ceará, Brazil

[e] Departamento de Ciências Biológicas, Faculdade de Ciências Exatas e Naturais, Universidade do Estado do Rio Grande do Norte,
59625-620, Mossoró, Rio Grande do Norte, Brazil

[f] Federal Institute of Education, Science and Technology of Ceara (IFCE), postal code 62930-000, Limoeiro do Norte-Ceará, Brazil

[g] Departamento de Física e Informática, Instituto de Física de São Carlos, Universidade de São Paulo, 13560-970, São Carlos, São Paulo, Brazil

[h] Biotechnology and Mass Spectrometry Research Group, Federal University of Ceará, 60440-900, Fortaleza, Ceará, Brazil

Supporting Figures and Table

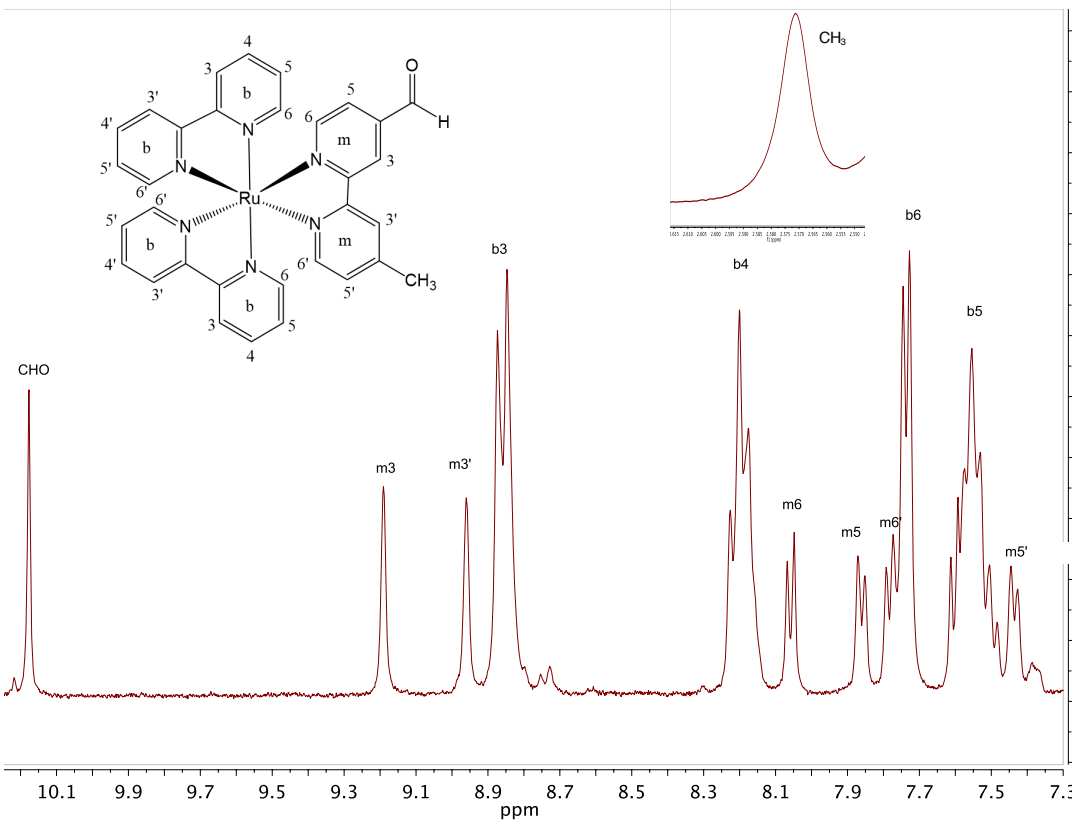

Figure S1. ^{1}H NMR spectrum of **Ru-CHO** (300 MHz, $(CD_3)_2SO$, 25 °C).

A

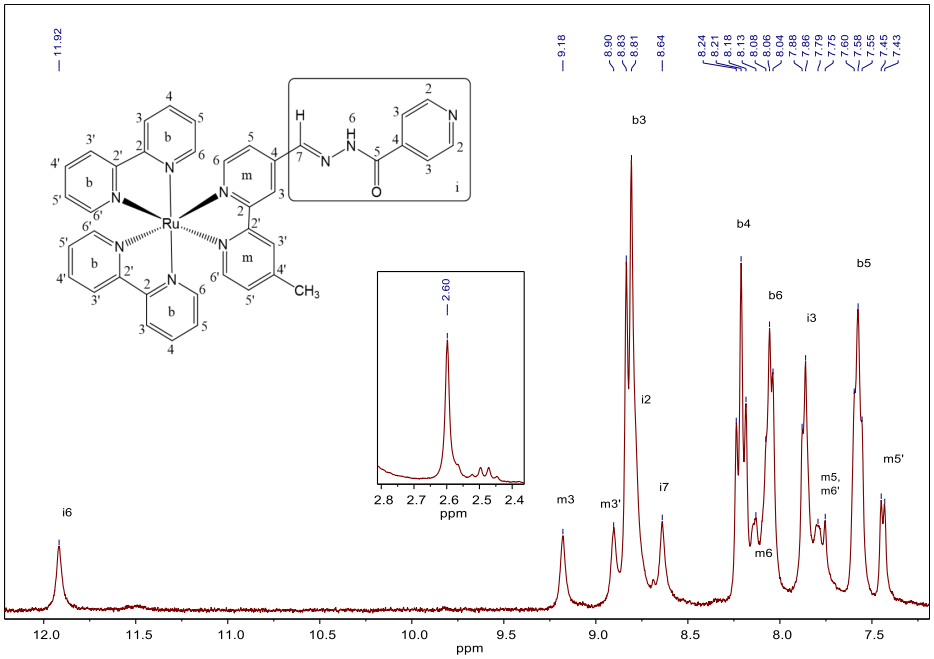

B

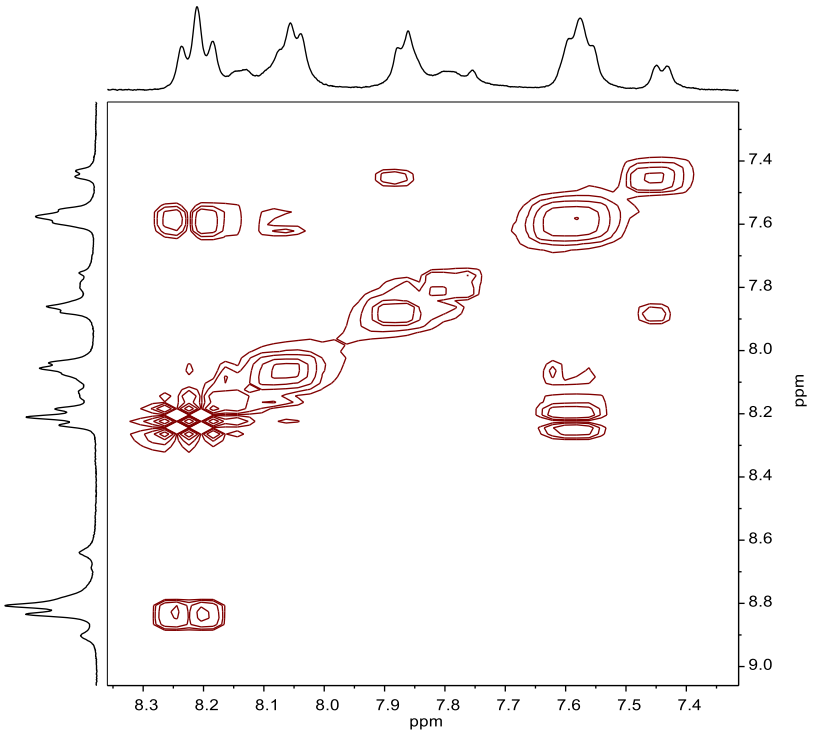

Figure S2. ^{1}H NMR spectrum of **Ru-INH,** 1-D (A) and 2-D (COSY) (B) (300 MHz, $CO(CD_3)_2$, 25 ºC).

S3A

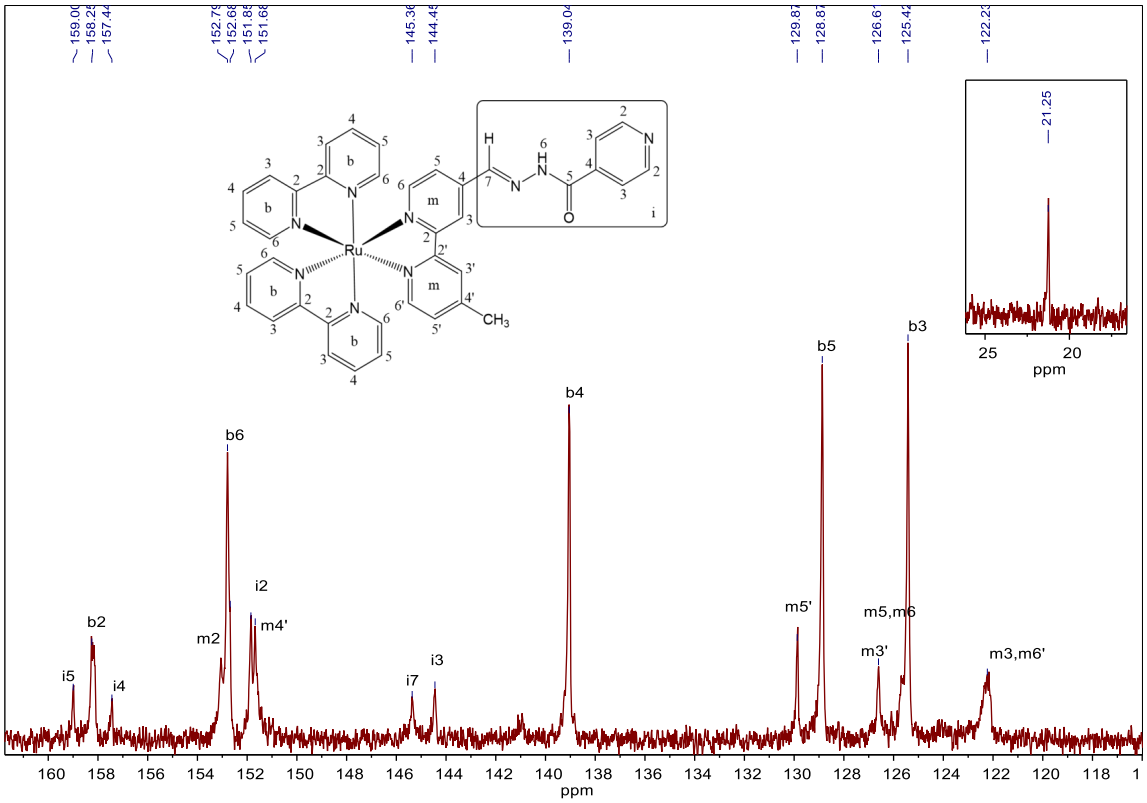
159.0
158.2
157.4
152.7
152.6
151.8
151.6
145.3
144.4
139.0
129.8
128.8
126.6
125.4
122.2
21.25
25
20
ppm
b3
b5
b4
b6
i2
m4'
b2
m2
i5
i4
i7
i3
m5'
m5,m6
m3'
m3,m6'
160
158
156
154
152
150
148
146
144
142
140
138
136
134
132
130
128
126
124
122
120
118
1
ppm

S3B

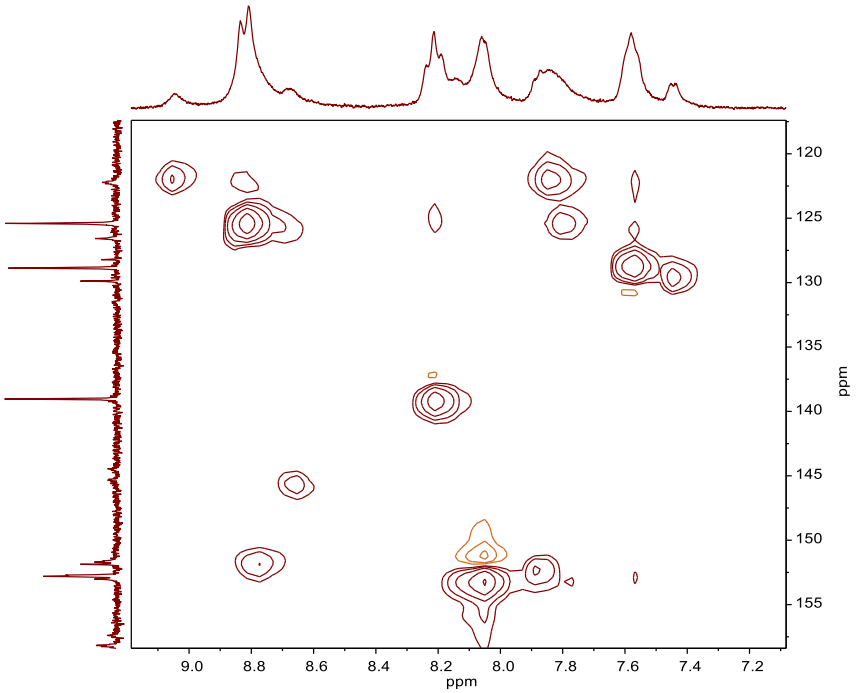
120
125
130
135
140
145
150
155
ppm
9.0
8.8
8.6
8.4
8.2
8.0
7.8
7.6
7.4
7.2
ppm

S3C

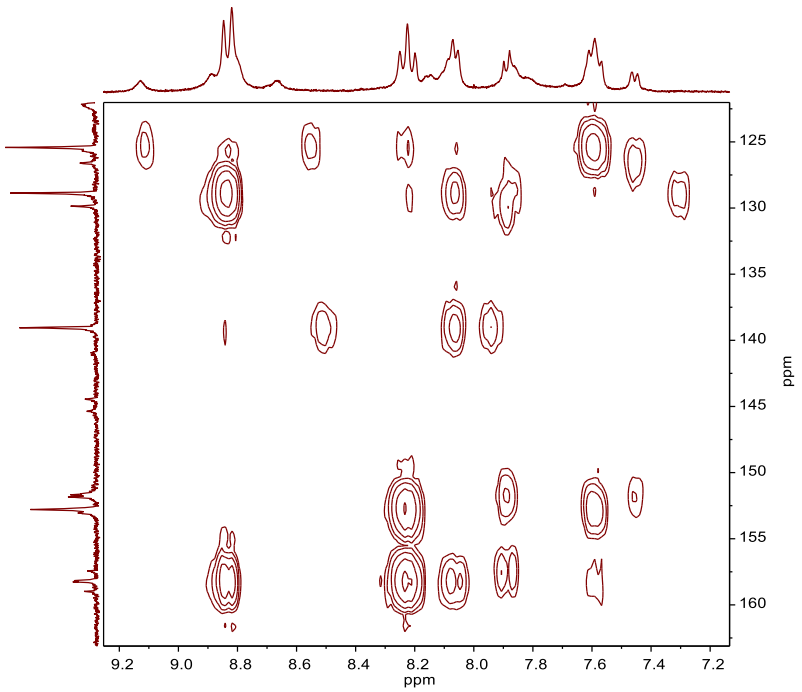

Figure S3. 1-D and 2-D ^{13}C NMR spectra of **Ru-INH** (100.63 MHz, $CO(CD_3)_2$, 25 ^oC), 1-D (A), 2-D (HSQC) (B) and 2-D (HMBC) (C).

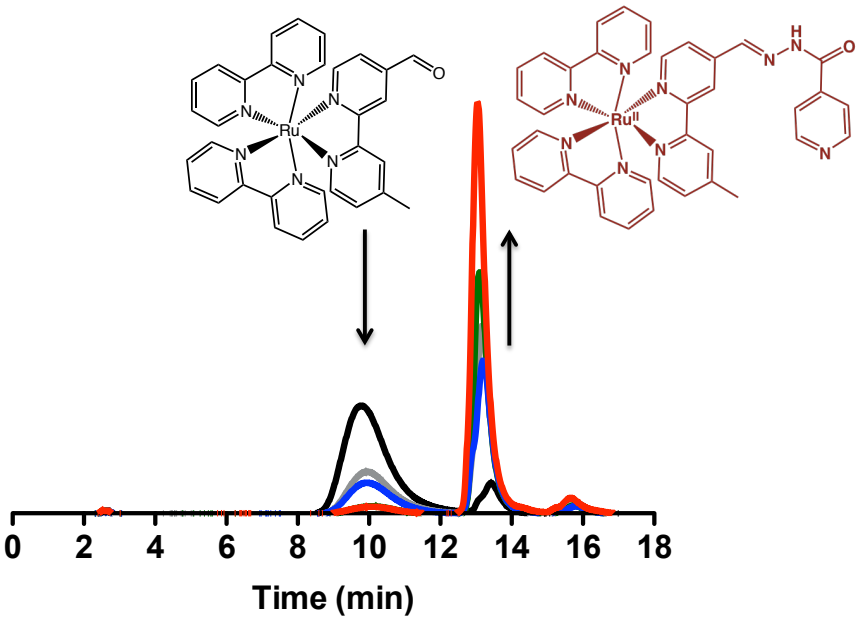

Figure S4. Chromatographic monitoring of the reaction of **Ru-CHO** with isoniazid (**INH**) for 7 h (gradient in acetonitrile from 20 – 50 %, C18 Bondapak column, 10 µm, Waters) at 450 nm (right after mixture t = 0 min (black); 1h (gray), 2h (blue), 5h (green) and 6h (red).

Figure S5. High-resolution mass spectrum of the isoniazid conjugated ruthenium(II) metal complex (**Ru-INH**) in methanol, expansion shown in the upper spectrum.

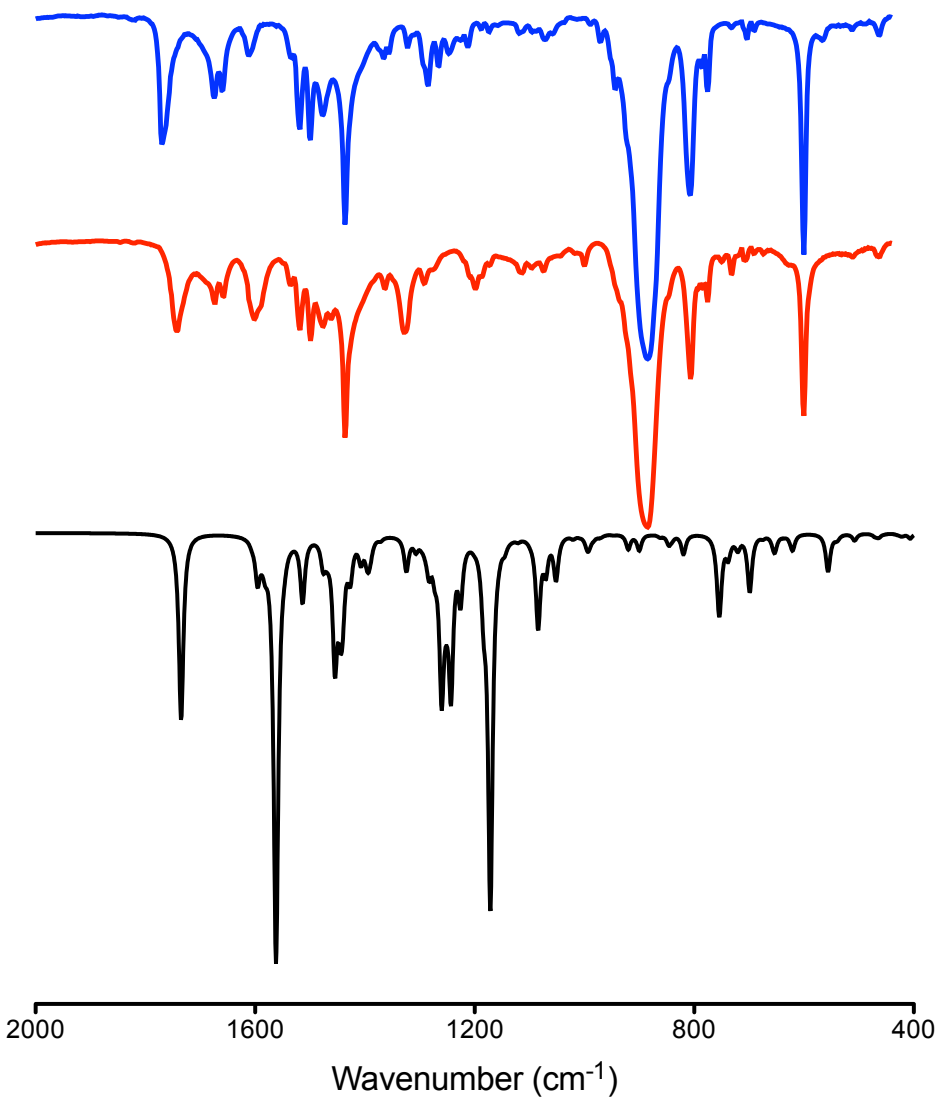

Figure S6. Infrared spectra of **Ru-CHO** (top, blue), **Ru-INH** (middle, red) in KBr pellet, and density functional theory (DFT) calculated spectrum of **Ru-INH** (bottom, black).

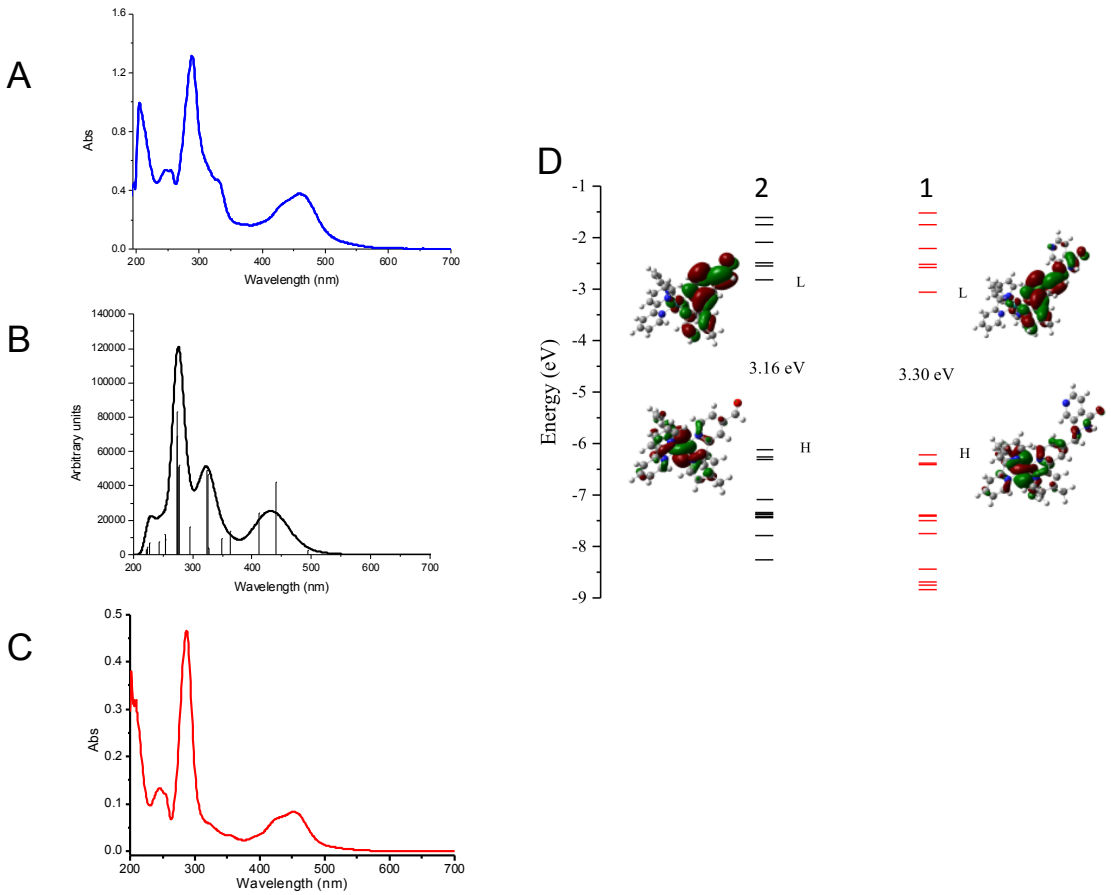

Figure S7. Electronic spectra for **Ru-INH** (A, experimental; B, time-dependent DFT (TD-DFT) calculated) and **Ru-CHO** (C), in methanol, (D) energy diagram as by TD-DFT (1 = **Ru-CHO**, 2 = **Ru-INH**) including the electron mappings of the highest occupied molecular orbital (HOMO) and lowest unoccupied molecular orbital (LUMO).

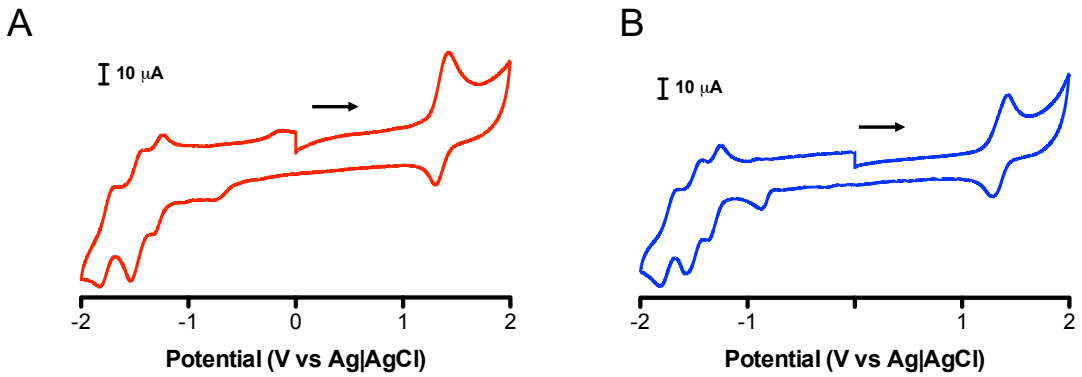

Figure S8. Cyclic voltammograms of a glassy-carbon at 0.1 V s^{-1} in acetonitrile containing 0.1 mol L^{-1} tetrabutylammonium perchlorate (PTBA) and **Ru-INH** (A) and **Ru-CHO** (B).

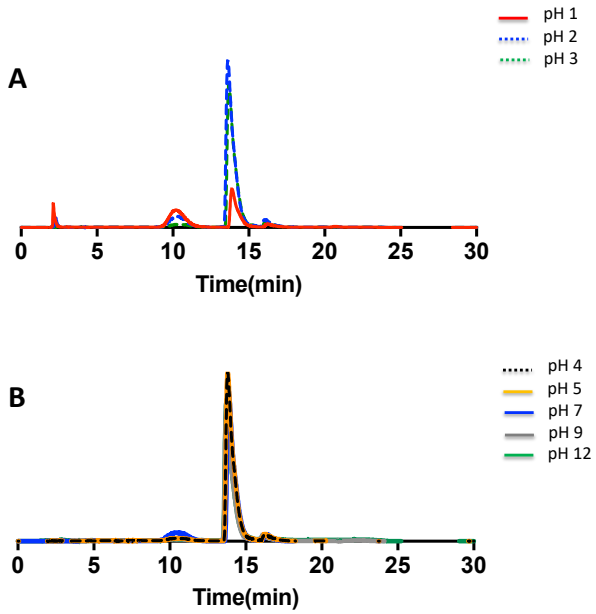

Figure S9. Chromatograms of **Ru-INH** complex incubated for 15h in aqueous solutions of pH values varying from 1 to 3 (Panel A) and 4 to 12 (Panel B) (acetonitrile/H_2O gradient from 20 – 50 %, C18 Bondapak column, 10 µm, Waters) monitored at 254 nm.

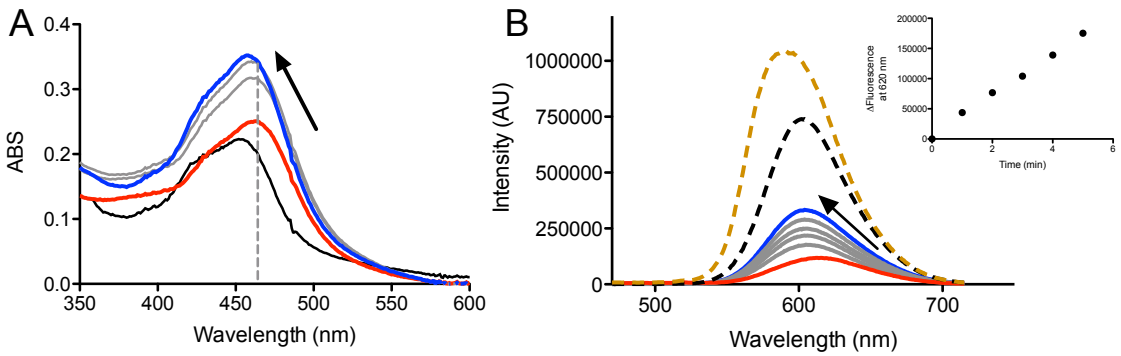

Figure S10. Effect of blue light on the electronic (A) and luminescence (B) spectra of **Ru-INH** in ethanol. Panel A shows the initial spectrum of **Ru-INH** (red) and spectral changes upon blue light irradiation toward the blue line (after 5 h). Black line stands for the **Ru-CHO** spectrum and the arrow indicates changes over time. Panel B shows the luminescence spectrum of **Ru-INH** (red) and spectral changes over time as indicated by the arrow reaching spectrum in blue after 5h. Dashed black and orange lines stand for **Ru-CHO** and **Ru-bpy** ($[Ru(bpy)_3]^{2+}$). Excitation at 450 nm.

Figure S11. High-resolution mass spectrometry for **Ru-INH** after 1 h of blue-light irradiation in methanol. Panel **A** shows **Ru-CHO** and **Ru-COOH**, and panel **B** shows a hemiacetal originated from **Ru-CHO.**

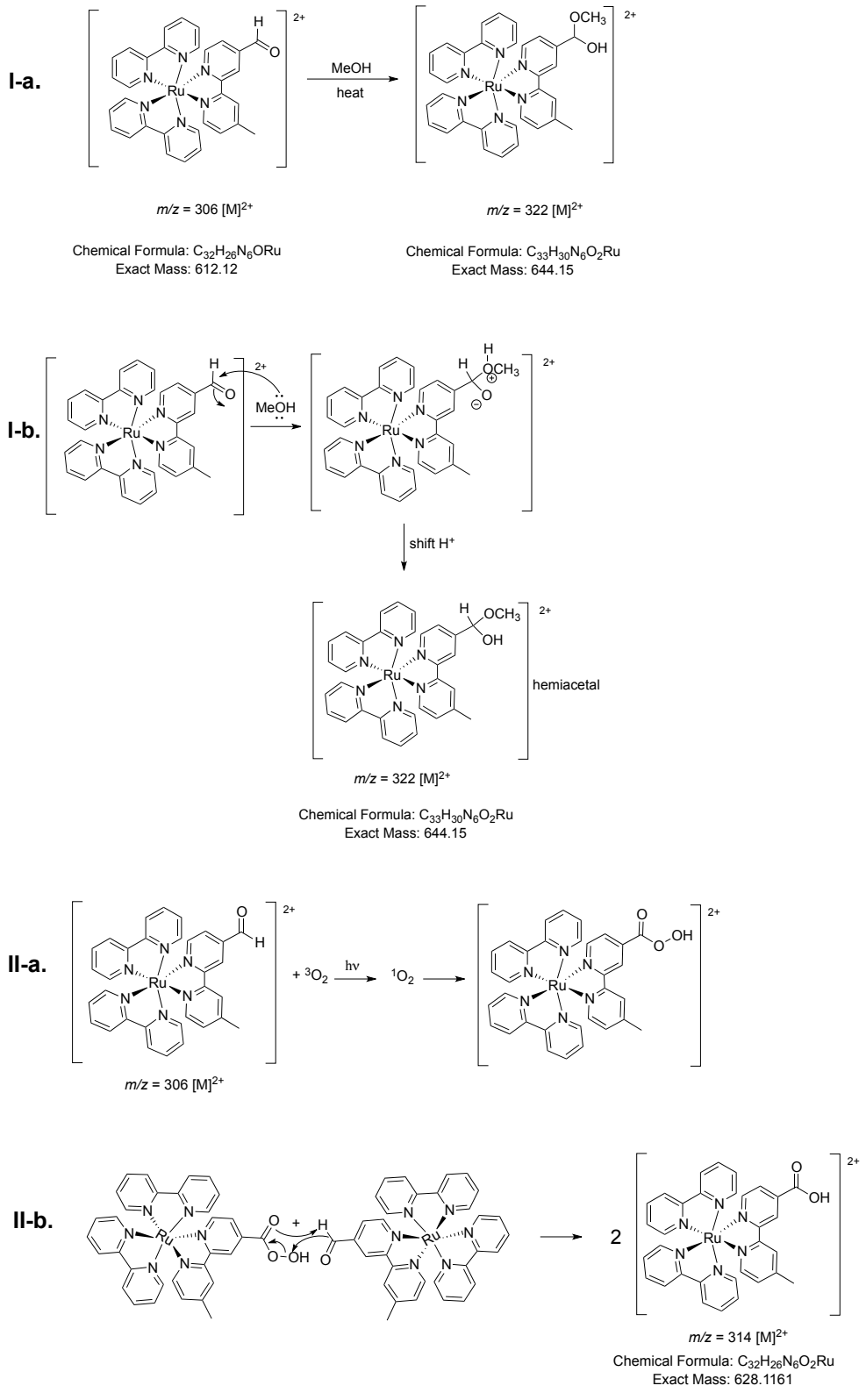

Figure S12. Proposed mechanism for the formation of **Ru-CHO** products observed by mass spectrometry (route I-a/b generated in the MS source; route II-a/b photochemically generated).

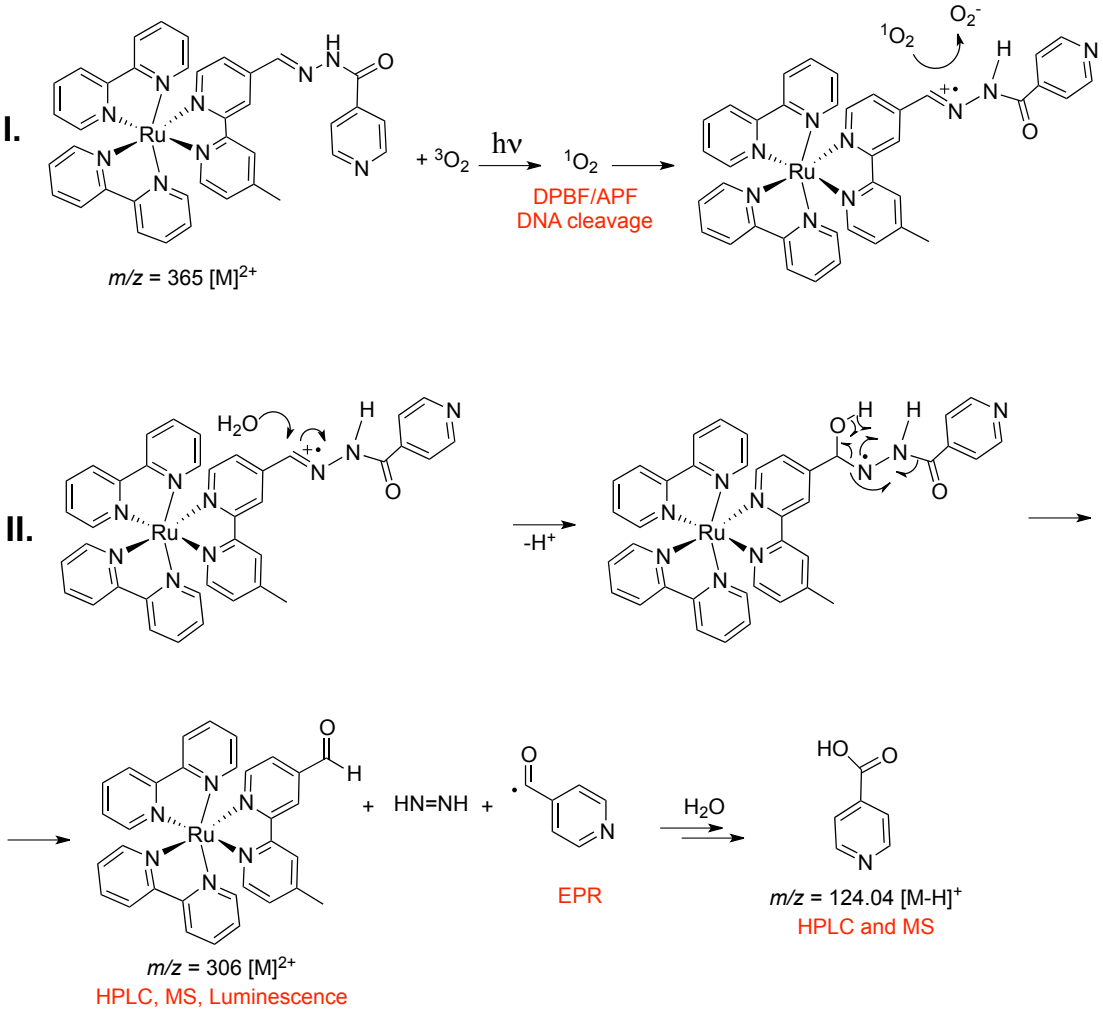

Figure S13. Proposed mechanism for light-induced oxygen-singlet disruption of **Ru-INH** complex (in red techniques used to support formation of products and intermediate).

Note: The **Ru-INH** complex was shown to be reasonably resistant to acid-base hydrolysis, but sensitive to blue light. Based on mass spectrometry, EPR and HPLC analysis, we proposed there is an initial oxidation of the acyl hydrazone by photogenerated singlet oxygen. This cation radical would have an eletronic rearrangment followed by the production of **Ru-CHO** complex and isonicotinoyl radical. Further later, the isonicotinoyl radical would originate the isonicotinic acid in analogy to the mechanism proposed for isoniazid activated by KatG or

manganese(III) pyrophosphate complex. We have experimental evidences supporting the formation of **Ru-CHO** either by HPLC and mass spectrometry, along with suggestive data from electronic absorption and luminescence studies of the photolysed complex (Fig. 3, 4 and Supporting Fig. S9).

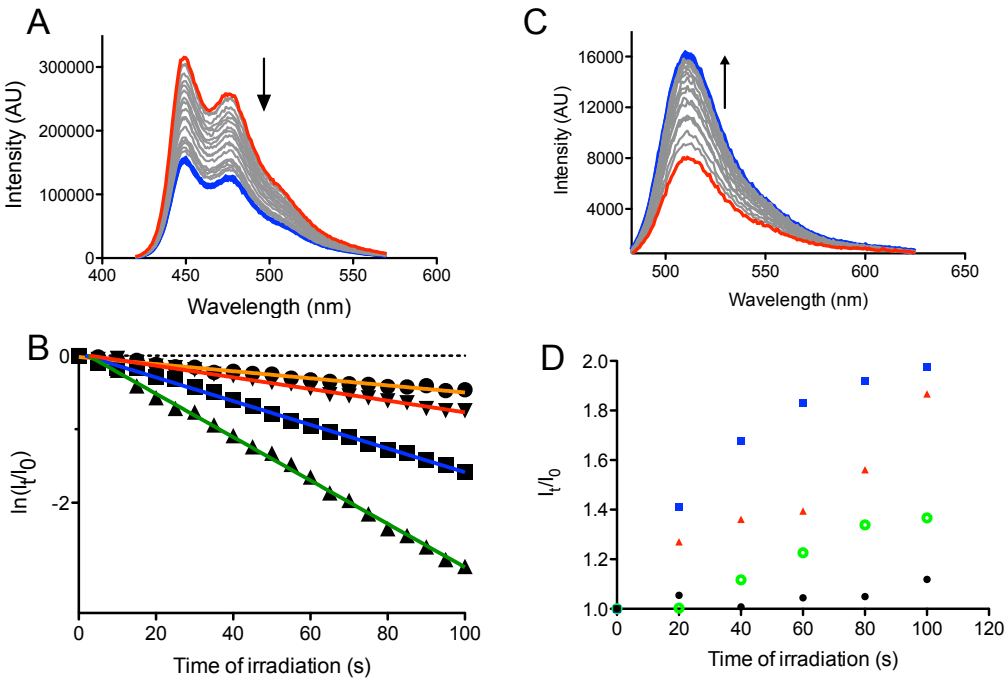

Figure S14. Investigation of radical oxygen species (ROS) photogeneration. Panel A shows the fluorescence spectra of the 1,3-diphenylisobenzofuran (DPBF) probe in ethanol with **Ru-INH** upon blue-light irradiation, while panel B exhibits a kinetic plot following the spectral changes of DPBF free of complexes (circles) and in the presence of **Ru-INH** (inverted triangles), **Ru-bpy** (triangle), **Ru-CHO** (squares). Panel C shows the fluorescence spectra of the aminophenyl fluorescein (APF) probe with **Ru-INH** upon blue-light irradiation in ethanol, while panel D exhibits a kinetic plot for the emission spectral changes of APF free of complexes (solid circles), and in the presence of **Ru-INH** (squares), **Ru-INH** and sodium azide (open circles), and **Ru-INH** and D-mannitol (triangles).

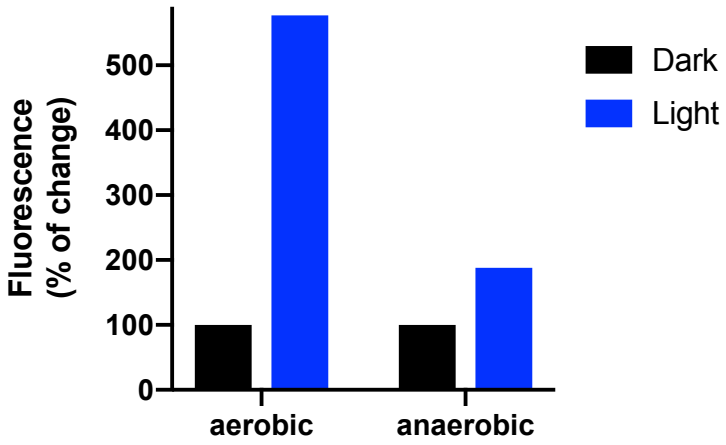

Figure S15. Effect of oxygen in the degradation of **Ru-INH** in ethanol, monitored by fluorescence intensity change at 618 nm, upon blue light irradiation (LED, 463 nm, 20 W) for 2h at 25 ^{o}C.

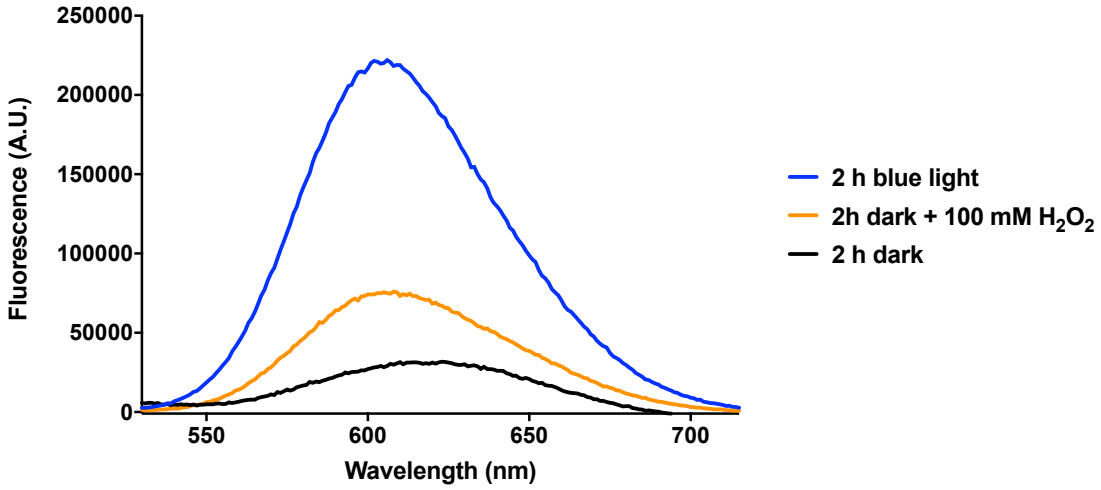

Figure S16. Comparative effect of blue light (blue line) and a large concentration of hydrogen peroxide (100 mmol L^{-1}, orange line) on **Ru-INH** disruption, monitored by fluorescence change after 2 hours. Complex protected of light shown in the black line.

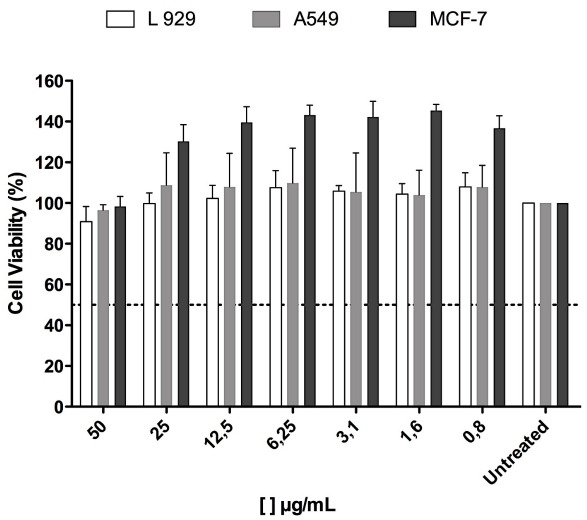

Figure S17. L 929, A549 and MCF-7 cell viability determined by MTS (([3-(4,5-dimethylthiazol-2-yl)-5-(3-carboxymethoxyphenyl)-2-(4-sulfophenyl)-2H-tetrazolium) assay after 48 h of treatment with **INH** in different doses, without blue light.

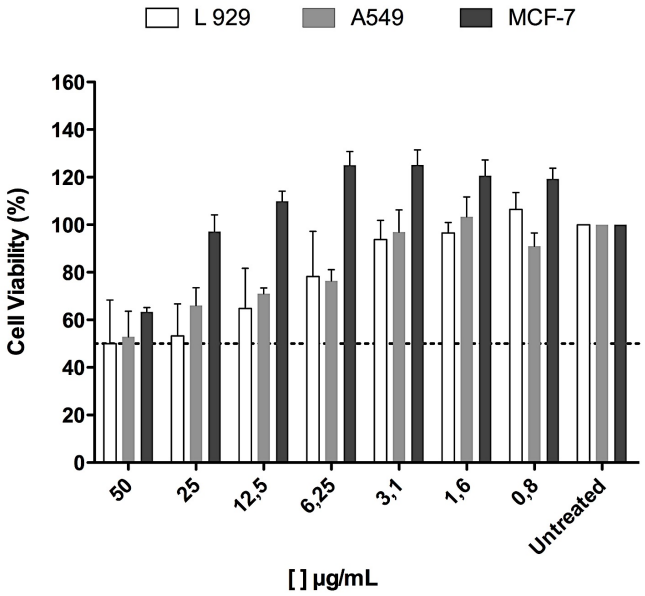

Figure S18. L 929, A549 and MCF-7 cell viability determined by MTS assay after 48 h of treatment with **INH** in different doses with blue light exposition.

Table S1. Calculated electronic absorptions of **Ru-COH** and **Ru-INH** metal complexes.

λ_{DFT} (nm)		λ_{EXP}	f	Major contribution	Assignment
Ru-COH	451	452	0.1392	H-2→LUMO (47%)	MLCT bpyR
	403	423	0.1283	H-2→L+1 (35%), H-1→L+2 (31%)	MLCT bpy
	314	324	0.1216	H-5→LUMO (39%), H-2→L+4 (26%)	ILbpyR, MLCT bpy
	295		0.1072	H-1→L+6 (34%)	MLCT bpy
	276	287	0.2782	H-4→L+2 (37%)	IL bpy
	274		0.7097	H-4→L+1 (25%), H-3→L+2 (32%)	IL bpy
	258	245	0.1083	HOMO→L+9 (43%)	MLCT bpyR
	256		0.202	H-5→L+3 (56%)	IL bpyR
	218		0.0552	H-8→L+2 (25%)	IL bpy
Ru-INH	493	520	0.0137	HOMO→LUMO (89%)	MLCT bpyR
	440	461	0.2392	H-1→LUMO (80%)	MLCT bpyR
	411	433	0.1364	H-2→L+1 (66%)	MLCT bpy
	325	329	0.2673	H-3→LUMO (41%)	IL bpyR
	323		0.2786	H-1→L+4 (49%)	MLCT bpy
	277	288	0.2973	H-7→L+2 (30%), H-6→L+2 (20%)	IL bpy
	275		0.2911	H-3→L+3 (54%)	IL bpyR
	274		0.395	H-4→L+1 (39%)	LLCT
	253	248	0.069	H-7→L+3 (50%)	IL bpyR
	243		0.0432	H-5→L+4 (65%)	IL bpy

MLCT = metal to ligand charge transfer electronic transition; IL = intraligand electronic transition; LLCT = ligand-to-ligand charge transfer electronic transition; bpy-R = mbpy-CHO or mbpy-INH